Radiative transfer in the earth's atmosphere and ocean: influence of ocean waves

Gilbert N. Plass, George W. Kattawar, and John A. Guinn, Jr.

The radiance in the earth's atmosphere and ocean is calculated for a realistic model including an ocean surface with waves. Individual photons are followed in a Monte Carlo calculation. In the atmosphere, both Rayleigh scattering by the molecules and Mie scattering by the aerosols as well as molecular and aerosol absorption are taken into account. Similarly, in the ocean, both Rayleigh scattering by the water molecules and Mie scattering by the hydrosols as well as absorption by the water molecules and hydrosols are considered. Separate single-scattering functions are used which are calculated separately for the aerosols and the hydrosols from the Mie theory with appropriate and different size distributions in each case. The scattering angles are determined from the appropriate scattering function including the strong forward-scattering peak when there is aerosol or hydrosol scattering. Both the reflected and refracted rays, as well as the rays that undergo total internal reflection, are followed at the ocean surface. The wave slope is chosen from the Cox-Munk distribution. Graphs show the influence of the waves on the upward radiance at the top of the atmosphere and just above the ocean surface and on the downward radiance just below the ocean surface as well as deeper within the ocean. The radiance changes are sufficient at the top of the atmosphere to determine the sea state from satellite measurements. Within the ocean the waves smooth out the abrupt transition that occurs at the edge of the allowed cone for radiation entering a calm ocean. The influence of the waves on the contrast between the sky and sea at the horizon is discussed. It is shown that the downward flux just below the surface increases with wind speed at all solar angles.

I. Introduction

Since the majority of the earth's surface is covered by water, it is important to have a realistic model of the multiple scattering of solar photons in an atmosphere–ocean system. Solar photons undergo absorption and multiple scattering by aerosols and atmospheric molecules, reflection and refraction at the ocean surface, and further absorption and multiple scattering by hydrosols and water molecules of the ocean. Additional complexity arises from scattering and absorption by the ocean floor and from refraction and reflection (including total internal reflection at some angles) of the upwelling light at the ocean boundary.

The scattering from the aerosols and hydrosols is asymmetric with strong forward scattering, since their size is of the same order as the wavelength of visible light. An accurate theory of the radiation field must take into account (1) the actual phase function of the aerosols and hydrosols; (2) the various scattering and absorption processes of the different aerosols, hydrosols, and molecules in the atmosphere and ocean; (3) all orders of multiple scattering of any significance; (4) the reflection and refraction of the radiation at the atmosphere–ocean interface, including the effect of the ocean waves.

Various techniques have been proposed to obtain numerical solutions of the equations of radiative transfer. One of the most successful has been the matrix operator theory which has been reviewed by Plass *et al.*[1] Accurate solutions can be obtained by this method for optically deep layers that may be inhomogeneous. Interior radiances can also be calculated by this method.[2,3] The method has not yet been used when there is a boundary such as the ocean surface that reflects and refracts light, although we are attempting such an extension. The method has also not been used for highly asymmetric phase functions because of the large number of Fourier terms required.

The Monte Carlo method is used here to solve the atmosphere–ocean problem. The basic method has been described by Plass and Kattawar.[4,5] The method was extended to calculate the flux and radiance in an atmosphere–ocean system.[6–8] The complete Stokes vector has also been calculated for the atmosphere–ocean system by Kattawar *et al.*[9] in order to obtain the polarization and ellipticity of the radiation.

The authors are with the Physics Department, Texas A&M University, College Station, Texas 77843.

Received 14 March 1975.

The only calculations of the radiance in an ocean with waves previously published is by Raschke.[10] Gordon and Brown[11] have used Monte Carlo techniques to compute the radiation flux in a calm ocean, but they assume an isotropic radiance distribution incident on the ocean instead of coupling the radiation fields of the atmosphere and ocean.

II. Method of Calculation

The method of calculation has been described by Kattawar *et al.*[9]; thus only a few of the more important details are given here. The atmosphere was divided into a number of layers with an appropriate aerosol and ozone concentration in each layer. The aerosols were represented by spherical particles with a real index of refraction of 1.55 and with radii number density proportional to r^{-4} for $r > 0.1$ μm and constant for $0.03 \le r \le 0.1$ μm. The aerosol single scattering phase matrix was calculated from Mie theory. The aerosol and ozone variations with height were taken from the tables of Elterman *et al.*[12]

At the atmosphere–ocean interface both the reflected and refracted rays (including the rays that undergo total internal reflection) were followed. When the surface was assumed to have waves, a wave-slope was chosen from the distribution found by Cox and Munk.[13] This part of the calculation is described in more detail, since it is new.

The Cox-Munk wave-slope distribution is that which a normally incident photon would see as it approaches the interface. Photons incident from other directions, however, see a distribution of wave-slopes which is a projection of the given distribution onto the plane normal to the incident direction of the photon, and the distribution must be adjusted accordingly (see Ref. 13, Sec. 4.2, for a related discussion).

Consider a patch of ocean of unit horizontal area at an instant in time in which every possible slope occurs (assuming, for simplicity, a discrete set). Assume that each slope is represented by a facet whose horizontally projected area is proportional to the probability of occurrence of that slope. This unit patch of ocean is thus representative of the surface as a whole.

If the probability that a vertically incident photon will strike some facet within the unit area is unity, the probability that such a photon will strike a facet with a particular slope equals the probability of occurrence of that slope. This probability—the horizontally projected area of the facet under consideration divided by the total (unit) area of the possible-interaction surface—must be modified when considering nonvertically incident photons, for the areas involved must be projected onto a plane perpendicular to the incident direction of each photon. Consider a photon whose direction of travel is inclined at an angle θ with respect to the vertical and a facet whose normal is similarly inclined at an angle θ_f. Assume that the angle between the incident direction of the photon and the facet normal—the incident angle—is θ_i. If the probability of occurrence of this facet is p, its actual area is $p/\cos_f$. The area seen by the incident photon would be $(p/\cos\theta_f)\cos\theta_i$. The probability of interaction of the photon and facet under consideration is therefore

$$p(\cos\theta_i)/(A\cos\theta_f),$$

where A is the sum of the similarly projected areas of all other facets capable of interaction with the given photon. (Properly excluded from the sum are facets on the back side of the wave—that is, facets that the photon cannot see because $\theta_i > \pi/2$. This exclusion due to facet orientation is to be distinguished from occultation, the hiding of the facets of one wave, regardless of orientation, by an adjacent wave. The current program does not take occultation into account.) For a sufficiently calm ocean the wave structure deviates little from the flat reference surface of the interface, so $A \approx \cos\theta$. In general, however, the sum must be carried out for each photon inclination angle. Note that for vertical incidence $A = 1$ and $\theta_i = \theta_f$, leaving the original probability p unmodified.

The hydrosols were represented by spheres with $n_1 = 1.15$ and $n_2 = 0.001$, where n_1 and n_2 are the real and imaginary parts, respectively, of the index of refraction with respect to water. The assumed size distribution is constant for $r < 1$ μm and proportional to $r^6\exp(-2r)$ for $r > 1$ μm, where r is the radius of the hydrosol. The calculations were made for the clear ocean model of Ref. 9. Two cross-section ratios are needed to specify the ocean model: σ_{ST}/σ_T and σ_{SR}/σ_{ST}, where σ_{ST} is the total scattering cross section, σ_{SR} the Rayleigh scattering cross section, and σ_T the total cross section for all processes. The first ratio determines the probability that the photon is scattered instead of being absorbed upon collision, while the second ratio determines the probability that a scattered photon undergoes Rayleigh instead of hydrosol scattering. Most of the calculations reported here were made for a wavelength $\lambda = 0.46$ μm, while some are for $\lambda = 0.70$ μm; the cross section ratios used for the ocean were $\sigma_{ST}/\sigma_T = 0.514$ and 0.0498 at $\lambda = 0.46$ μm and 0.70 μm, respectively, and $\sigma_{SR}/\sigma_{ST} = 0.218$ and 0.0494. The ocean was assumed to have an optical depth (defined as the product of the number density, total cross section, and vertical distance from ocean surface) $\tau = 10$ in all cases with a totally absorbing surface at the bottom. This latter assumption could only influence the radiance values near the bottom, but not those near the atmosphere–ocean surface because of the large optical depth.

A typical computer run took between 9 min and 14 min on the CDC 7600 during which time between 1.4×10^6 and 1.9×10^6 collisions were processed. The results of a single run give the upward and downward radiance and flux for eleven different detectors, which are located at various heights from the top of the atmosphere to the bottom of the ocean.

III. Radiance

The radiance was calculated for several different solar zenith angles and wind speeds. The only aver-

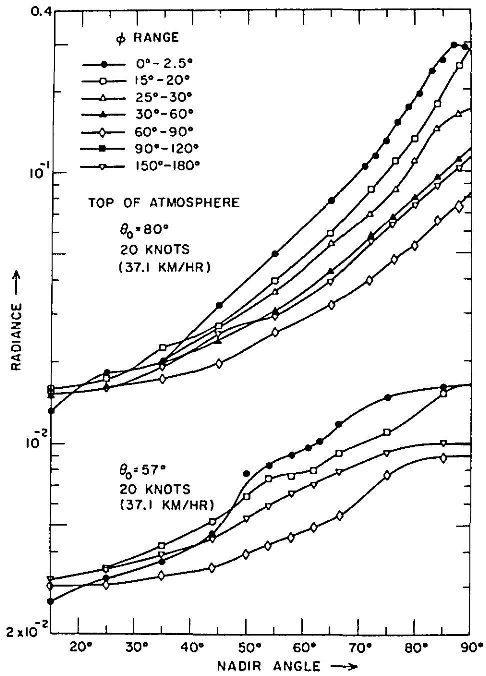

Fig. 1. Upward radiance at top of atmosphere as a function of nadir angle of observation for $\theta_0 = 57°$ and 80° (solar zenith angle), $\lambda = 0.46$ μm, and a wind speed of 20 knots (37.1 km/h). Each curve is averaged over a range of azimuthal angles ϕ as shown in the legend.

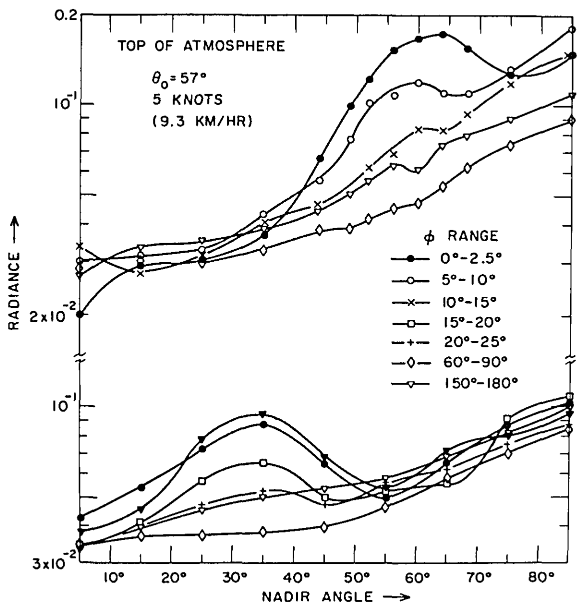

Fig. 2. Upward radiance at top of atmosphere for $\theta_0 = 32°$ (lower curves) and 57° and a wind speed of 5 knots (9.3 km/h).

aging done in the Monte Carlo method is at the detectors, which record the photons that arrive over various chosen intervals of solid angle. The solid angle seen by the detectors was varied with θ (the zenith or nadir angle) and ϕ (the azimuthal angle); the angular intervals were chosen smaller in the regions where the curve varied the most rapidly.

The upward radiance as seen at the top of the atmosphere is shown in Fig. 1 for a solar zenith angle $\theta_0 = 80°$ (top curves) and $\theta_0 = 57°$ (lower curves). The wind speed is assumed to be 20 knots (37.1 km/h). A wavelength of 0.46 μm was chosen for most of these calculations as this is near the wavelength for maximum transmission in the ocean. The radiance is shown as a function of the nadir angle of observation. Each curve is for a particular range of the azimuthal angle ϕ, as indicated in the legend. In all graphs in this article each symbol represents a calculated point. All Monte Carlo results have an experimental error due to statistical fluctuations. A curve has been drawn in every case by hand through the calculated points in order to guide the eye. In drawing the curve various information was used such as the shape of curves for neighboring values of the parameters and in some cases the values of calculated points that are off the scale of the graph. The curves have no other significance, and in some cases the reader may wish to draw his own curves through the calculated points. In each case the radiance is shown in the principal plane ($0° \leq \phi \leq 2.5°$) as well as for several other azimuthal angles. The curves for additional azimuthal angles were drawn only if they were significantly different from the previous curves. In all cases the calculated radiance should agree with a measured value averaged over a sufficiently long time interval to eliminate sudden intensity changes from the glitter.

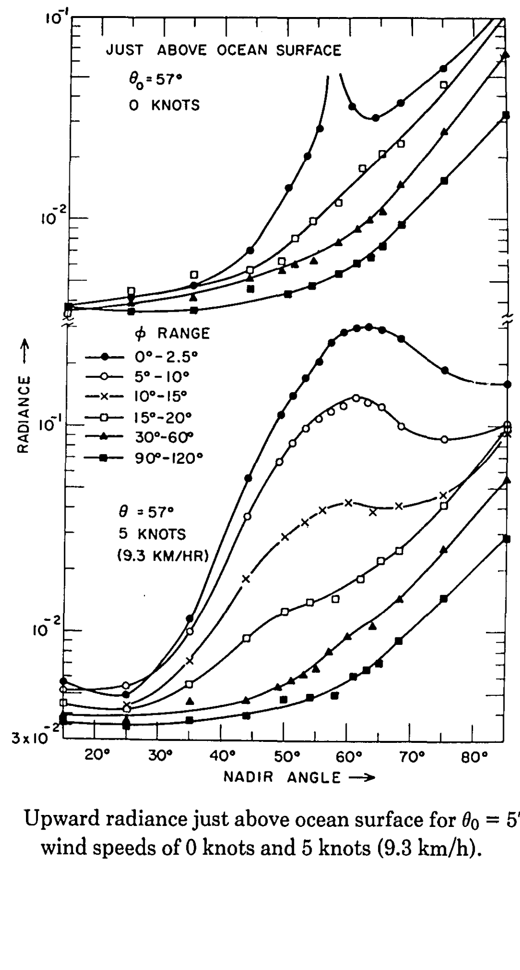

Fig. 3. Upward radiance just above ocean surface for $\theta_0 = 57°$ and wind speeds of 0 knots and 5 knots (9.3 km/h).

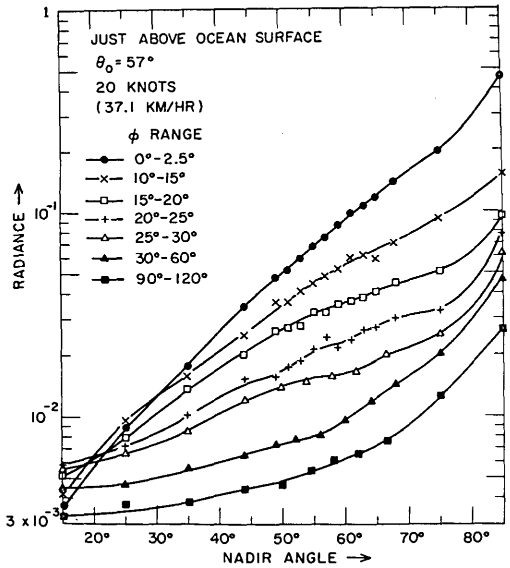

Fig. 4. Upward radiance just above ocean surface for θ_0 = 57° and a wind speed of 20 knots (37.1 km/h).

The radiance at the top of the atmosphere for a wind speed of 5 knots (9.3 km/h) is given in Fig. 2 for θ_0 = 57° and 32°. The radiance on a given almucanter (fixed nadir angle) is usually a maximum in the principal plane with ϕ = 0°. When there is a calm ocean the radiance as seen at the top of the atmosphere has a maximum value near the angle for specular reflection from the ocean. The atmospheric scattering slightly diffuses this radiation around this direction. The waves further diffuse this radiation as can be seen by comparing the curves for θ_0 = 57° at 5 knots and 20 knots in Figs. 1 and 2. There is still a maximum in the radiance curve near a nadir angle of θ = 60° for $0° \leq \phi \leq 2.5°$ at 5 knots, but this has largely disappeared at 20 knots. Furthermore the waves have scattered the direct solar image into the neighboring ϕ ranges. Appreciable differences in the radiance can be observed from space as the wind speed varies.

Because of the change in the upward radiance between the ocean surface and the top of the atmosphere due to the multiple scattering effects of the atmosphere, it is more instructive to study the upward radiance just above the ocean surface. This is shown in Figs. 3–5. The upward radiance for θ_0 = 57° is given in Figs. 3 and 4 for wind speeds of 0 knots, 5 knots, and 20 knots (0 km/h, 9.3 km/h, and 37.1 km/h). The radiance for $0° \leq \phi \leq 2.5°$ shows a sharp maximum around the specular angle of 57° for a calm ocean, a much broader maximum centered at about 63° for a 5-knot wind, and virtually no trace of a maximum when there is a 10-knot (data not shown) or 20-knot wind. There is also an appreciable maximum in the radiance curves for azimuths up to 15° for a 5-knot wind, but none at all for the 20-knot case. The curves for azimuths near 90° change little with the wind speed.

The radiance for θ_0 = 32° is given in Fig. 5 for 0-knot and 5-knot winds. Once again the moderate 5-knot wind spreads out the maximum, which occurs at the specular angle for a calm ocean, in both the polar and azimuthal angle. Data not given here show that there is still a weak maximum for a 10-knot wind speed, but that it has completely disappeared for a 20-knot speed.

The influence of the waves on the downward radiance just below the ocean surface is illustrated in Figs. 6–13. The variation of the radiance with zenith angle is given in Figs. 6 and 7 for a calm ocean and for θ_0 = 80°, 57°, and 32°. In all cases there is a sharp

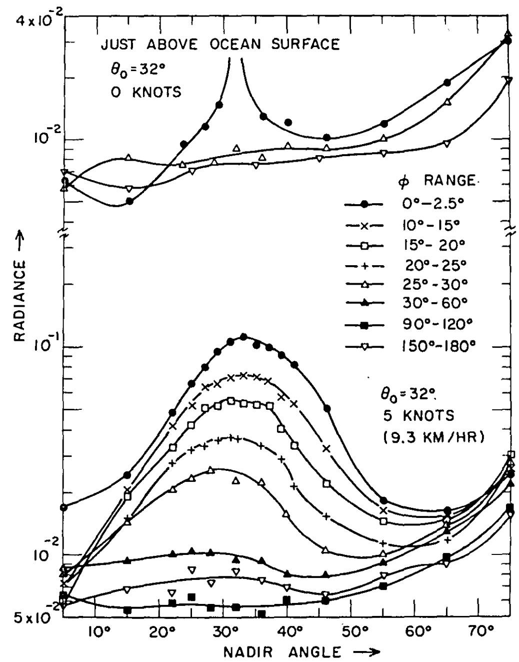

Fig. 5. Upward radiance just above ocean surface for θ_0 = 32° and wind speed of 0 knots and 5 knots (9.3 km/h).

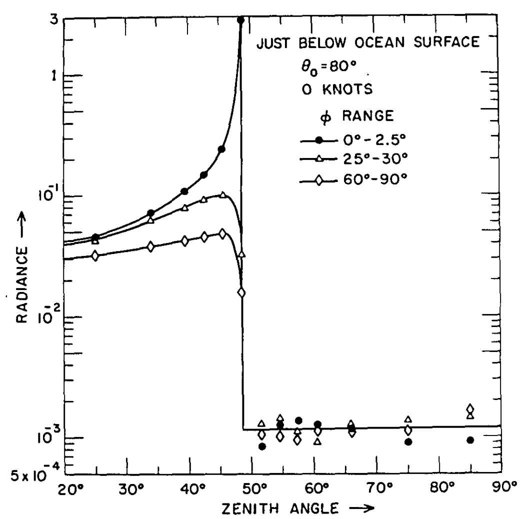

Fig. 6. Downward radiance just below ocean surface as a function of zenith angle of observation for θ_0 = 80° and a wind speed of 0 knots.

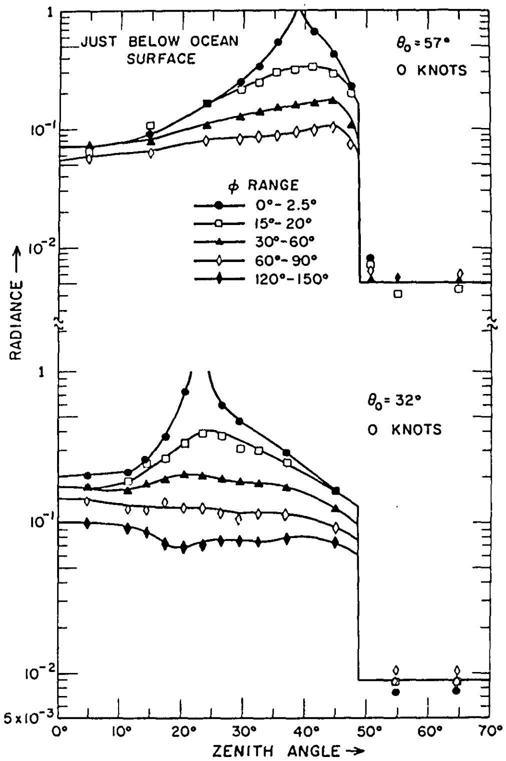

Fig. 7. Downward radiance just below ocean surface for θ_0 = 32° and 57° and a wind speed of 0 knots.

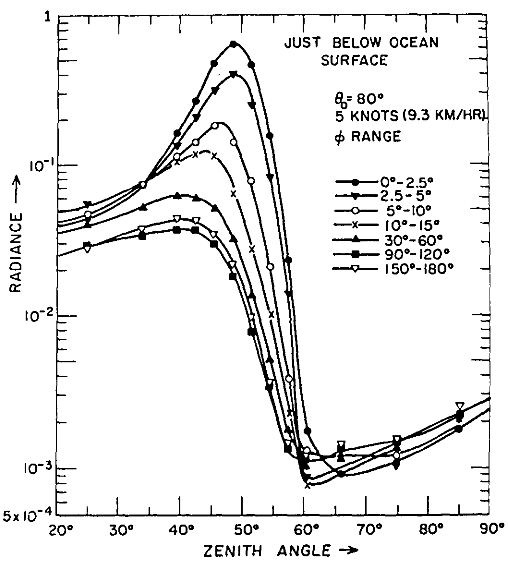

Fig. 8. Downward radiance just below ocean surface for θ_0 = 80° and a wind speed of 5 knots (9.3 km/h).

decrease of 1 or 2 orders of magnitude in the value of the radiance at a zenith angle of 48.4°. All the incoming light from the sun and sky after it has undergone refraction at the ocean surface is within a cone whose axis is pointed toward the zenith and with an angle of 48.4°. The low radiance levels recorded at larger zenith angles are due to photons traveling upward in the ocean that are totally internally reflected at the ocean surface. The radiance in the principal plane has a maximum near the position of the refracted solar image. The radiance for azimuthal angles out to approximately 20° also has a maximum at approximately the same zenith angle.

The radiance for these same three solar zenith angles is shown in Figs. 8–10 for a wind speed of 5 knots (9.3 km/h). The radiance distribution is broadened near the maximum as the waves spread out the position of the refracted solar image. Furthermore, the sudden decrease of the radiance at the critical angle of 48.4° is now smoothed out by the action of the waves. The low values of the radiance typical of the

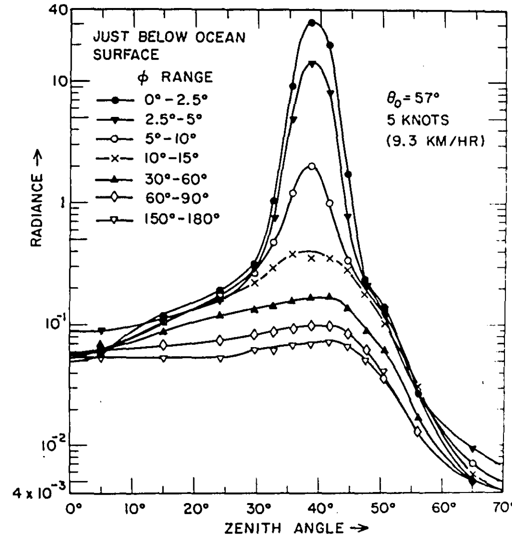

Fig. 9. Downward radiance just below ocean surface for θ_0 = 57° and a wind speed of 5 knots (9.3 km/h).

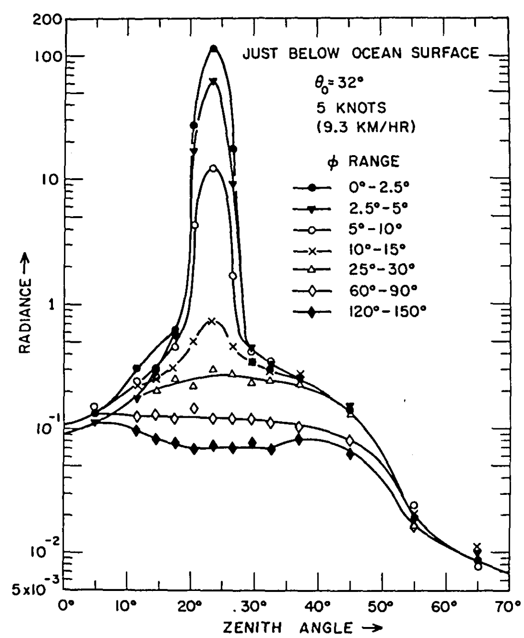

Fig. 10. Downward radiance just below ocean surface for θ_0 = 32° and a wind speed of 5 knots (9.3 km/h).

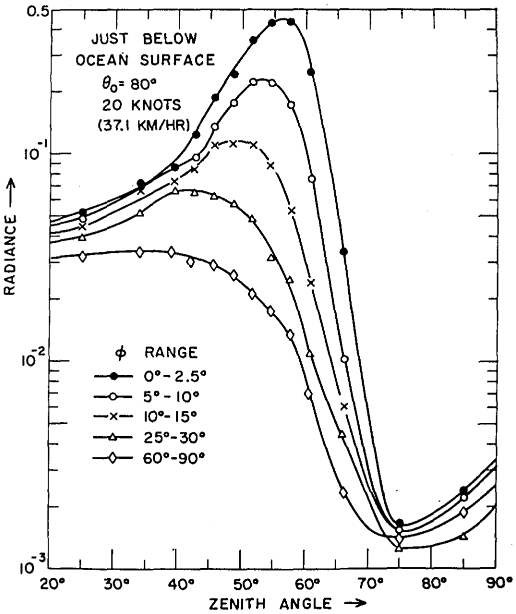

Fig. 11. Downward radiance just below ocean surface for $\theta_0 = 80°$ and a wind speed of 20 knots (37.1 km/h).

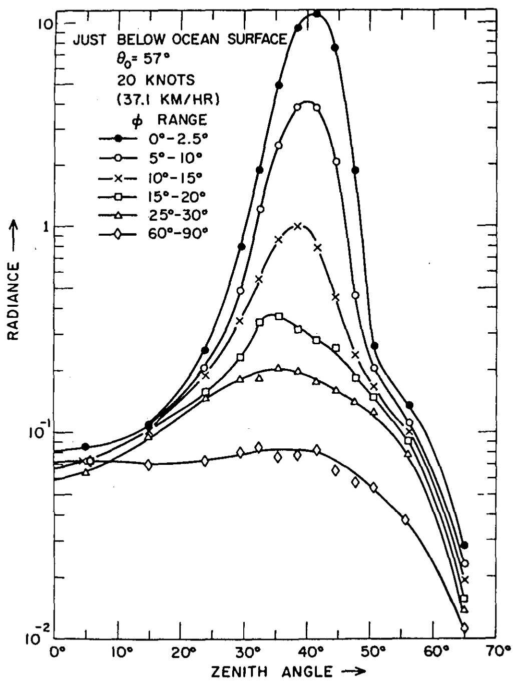

Fig. 12. Downward radiance just below ocean surface for $\theta_0 = 57°$ and a wind speed of 20 knots (37.1 km/h).

zone that cannot see the sky and sun ($\theta > 48.4°$) when the ocean is calm occur only for zenith angles greater than approximately 60° at this wind speed.

The same radiance curves, but for a wind speed of 20 knots (37.1 km/h), are shown in Figs. 11–13. The same features already described are even more obvious at the higher wind speed. The maxima are still broader, and the radiance curve does not reach the low values typical of the zone that receives no sky or direct sun radiation when the ocean is calm until the zenith angle increases to about 70°.

IV. Contribution of Direct Solar Beam

The case when the sun is at the zenith ($\theta_0 = 0°$) is illustrated in Figs. 14–16. These curves are for the principal plane only ($0° \leq \phi \leq 2.5°$). In order to understand better the various contributions to the light field, both the direct plus diffuse radiation and the

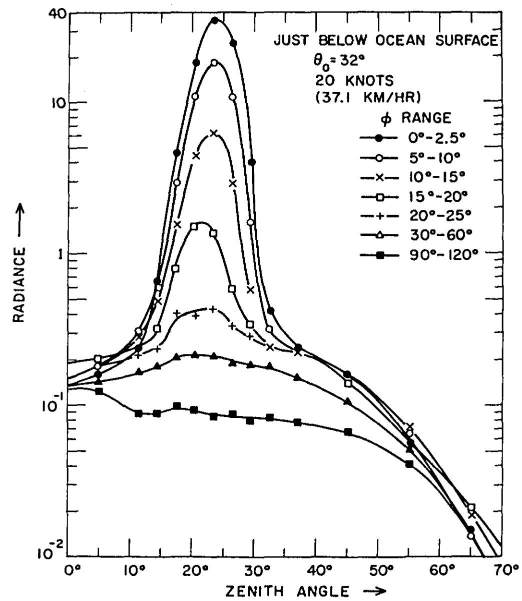

Fig. 13. Downward radiance just below ocean surface for $\theta_0 = 32°$ and a wind speed of 20 knots (37.1 km/h).

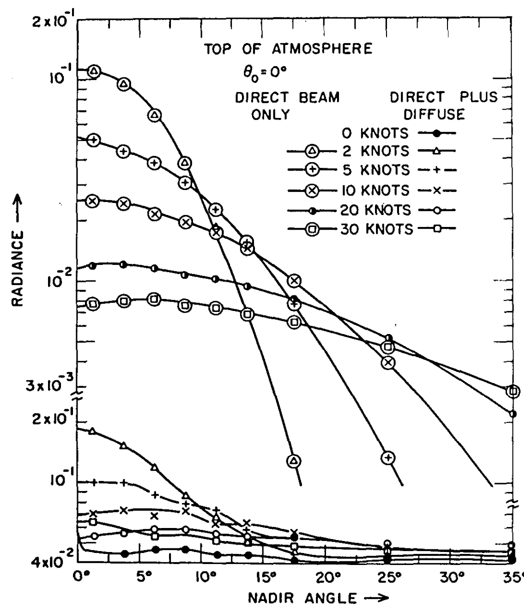

Fig. 14. Upward radiance at top of atmosphere as function of nadir angle of observation for $\theta_0 = 0°$ and the principal plane. Curves are given for six wind speeds from 0 knots to 30 knots. The upper curves are for the direct solar beam only. The lower curves show the total (direct plus diffuse) radiance.

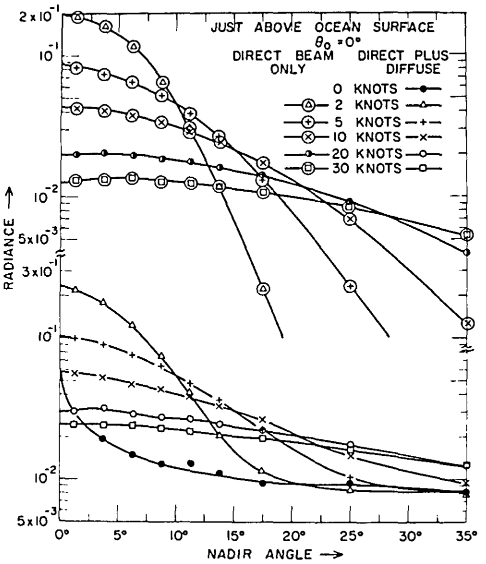

Fig. 15. Upward radiance just above ocean surface for $\theta_0 = 0°$ and the principal plane. See legend for Fig. 14.

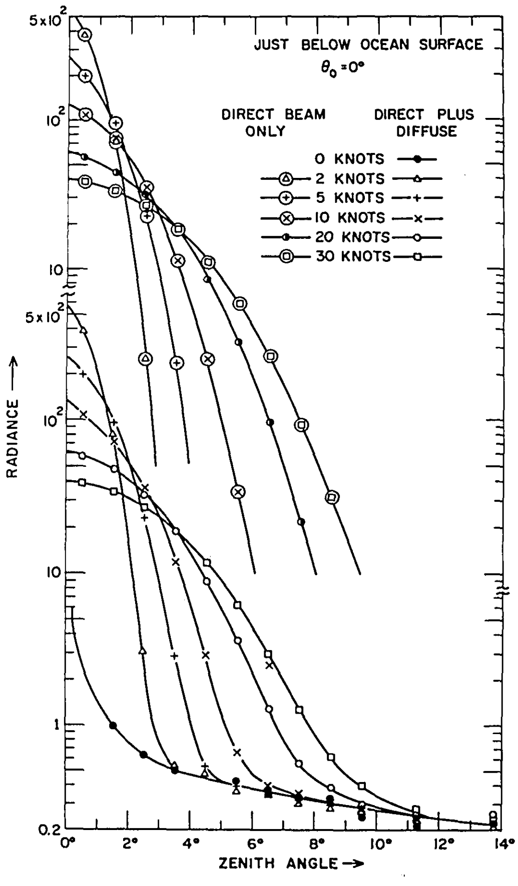

Fig. 16. Downward radiance just below ocean surface as function of zenith angle of observation for $\theta_0 = 0°$ and the principal plane. See legend for Fig. 14.

contribution from the direct solar beam only are shown. A photon is counted in the direct solar beam if it has not been scattered by a molecule, aerosol, or hydrosol. A photon in the direct solar beam for the upward radiance either at the top of the atmosphere or just above the ocean surface has been reflected at the ocean surface (but not scattered anywhere). Similarly the photon has been refracted at the ocean surface (but not scattered anywhere) if it is in the direct solar beam for the downward radiance just below the ocean surface. Curves are given for six different wind speeds in each of these figures.

At the top of the atmosphere (Fig. 14) the direct solar beam even at the nadir never contributes more than 60% of the total radiance. At larger nadir angles the contribution of the direct beam falls off rap-

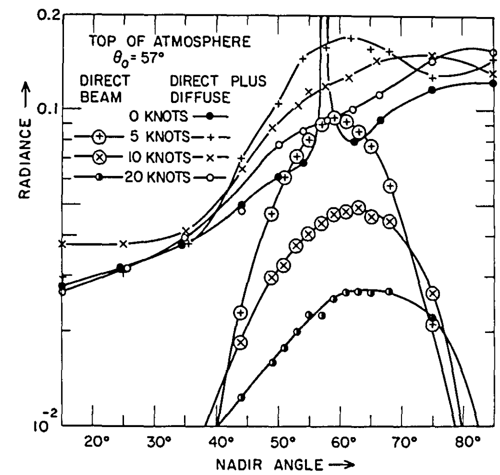

Fig. 17. Upward radiance at top of atmosphere as function of nadir angle of observation for $\theta_0 = 57°$ and the principal plane. Curves are given for four wind speeds from 0 knots to 20 knots. The lower curves are for the direct solar beam only. The upper curves show the total (direct plus diffuse) radiance.

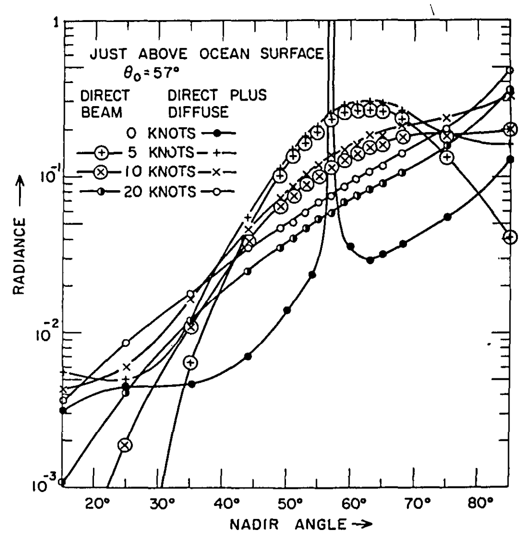

Fig. 18. Upward radiance just above ocean surface for $\theta_0 = 57°$ and the principal plane. See legend for Fig. 17.

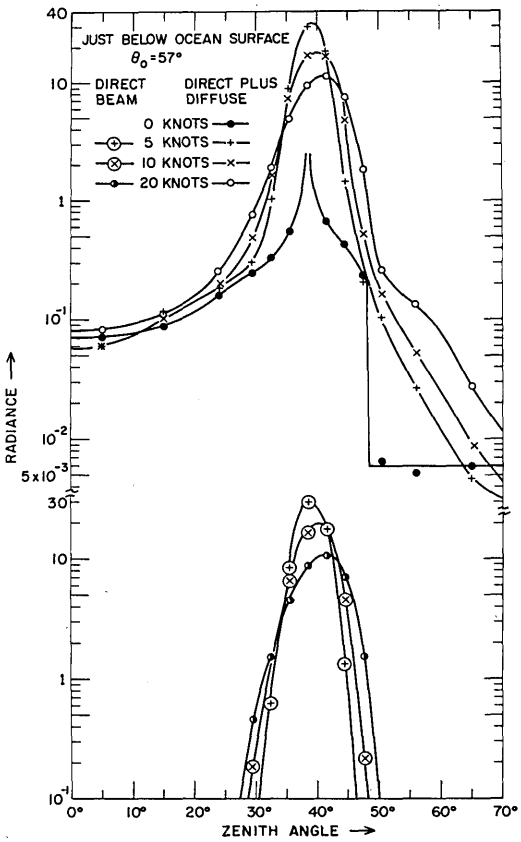

Fig. 19. Downward radiance just below ocean surface as function of zenith angle of observation for $\theta_0 = 57°$ and the principal plane. See legend for Fig. 17.

idly at all wind speeds. The total (direct plus diffuse) radiance has a maximum at the nadir that decreases as the wind speed increases. The maximum value for the radiance is approximately 0.18, 0.10, 0.070, and 0.052 for wind speeds of 2 knots, 5 knots, 10 knots, and 20 knots, respectively. The value of the radiance together with its variation with angle could be used to measure wind speed from space.

Just above the ocean surface (Fig. 15) the direct solar beam makes a much larger contribution to the total radiance for angles near the nadir. A comparison of Figs. 14 and 15 indicates how much the intensity of the direct solar beam is reduced in traveling from the ocean surface back to the top of the atmosphere; at the same time the total radiance is increased by photons that are scattered into the angle of observation by the atmosphere between these same two detectors.

Just below the ocean surface (Fig. 16) the direct solar beam is the major contributor to the total radiance at a wind speed of 30 knots out to a zenith angle of about 8°. At smaller wind speeds the direct beam decreases much more rapidly with zenith angle. The value of the radiance at the zenith varies from about 560 for a wind speed of 2 knots to 40 for a wind speed of 30 knots. The width of the radiance at one-tenth maximum is about 1.6° for a 2-knot wind and 6.2° for a 30-knot wind.

A similar set of curves for the radiance in the principal plane, but for a solar zenith angle of $\theta_0 = 57°$, is given in Figs. 17–19. At the top of the atmosphere (Fig. 17) the direct solar beam contributes 57% of the total radiance for a 5-knot wind and 26% of the total for a 20-knot wind. However, there is still an appreciable variation of the radiance with the wind speed at a nadir angle of 57°, since it decreases from 0.16 to 0.092 as the wind speed increases from 5 knots to 20 knots.

The upward radiance just above the ocean surface is shown in Fig. 18. In this case the direct beam makes the major contribution to the radiance over a wide range of angles around the specular angle of 57°. The direct beam contributes more than half of the total radiance for nadir angles from 35° to 80° for a 5-knot wind speed and from 30° to 90° for a 20-knot wind. The radiance curve still has a strong maximum (at about 63°) for the 5-knot wind; there is only a suggestion of the maximum in the curve for a 10-knot wind and no trace of the previous maximum for the 20-knot wind.

Just below the ocean surface (Fig. 19) the refracted solar beam for a calm ocean and $\theta_0 = 57°$ is at 38.8°. The sharp maximum in the downward radiance is near a zenith angle of 38.8°. As expected there is a sudden decrease in the radiance at 48.4° for a calm ocean as shown in this figure. The radiance curves at other windspeeds up to 20 knots still have strong maxima near 38.8° and illustrate how the wind smooths out the discontinuity at 48.4°. The direct beam makes a contribution of at least one-half of the total radiance from 31° to 45° when the wind speed is 5 knots and from 27° to 49° when the wind speed is 20 knots.

V. Radiance at 0.70 μm

All the results reported so far have been for a wavelength of 0.46 μm. The radiance at $\lambda = 0.70$ μm is shown in Figs. 20–22. Calculations were only done for wind speeds of 0 knots, 10 knots, and 20 knots at

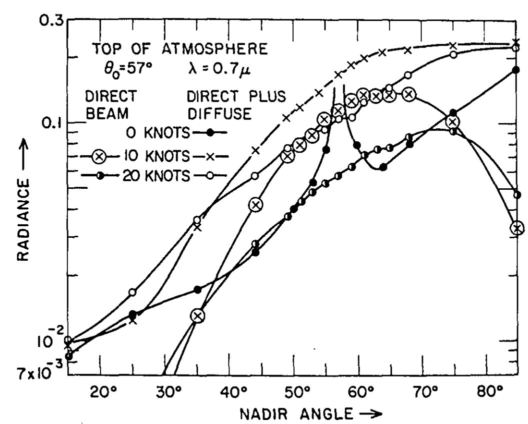

Fig. 20. Upward radiance at top of atmosphere as function of nadir angle of observation for $\theta_0 = 57°$, $\lambda = 0.7$ μm, and the principal plane. Curves are given for three wind speeds from 0 knots to 20 knots. The lower curves are for the direct solar beam only. The upper curves show the total (direct plus diffuse) radiance.

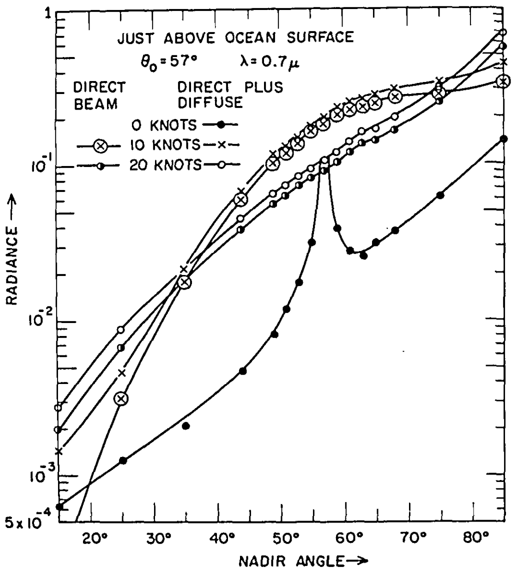

Fig. 21. Upward radiance just above ocean surface for $\theta_0 = 57°$ and the principal plane. See legend for Fig. 20.

this new wavelength. The radiance at the top of the atmosphere is given in Fig. 20. The direct beam makes a much larger contribution to the total at the new wavelength; this would be expected, since there is much less Rayleigh scattering in the red than in the blue. Thus the added contribution from atmospheric scattering is much less in the red. The difference in the radiance curves near a nadir angle of 57° for 10-knot and 20-knot winds is greater at the red wavelength than at the blue, which suggests that it may be easier to measure changes in the sea state from satellites at wavelengths around 0.7 μm.

The radiance in the red just above the ocean surface (Fig. 21) is determined largely by the reflected direct solar beam over a wide range of nadir angles.

Just below the ocean surface (Fig. 22) the main difference between the downward radiance at these red and blue wavelengths is the sudden drop by 3 orders of magnitude in the radiance curve at the red wavelength for a still ocean at the critical angle of 48.4° compared to a drop of only 1 order of magnitude at the blue wavelength. The upward radiance is much less in the red than in the blue due to greater absorption in the ocean. Thus the downward radiance just below the ocean surface outside of the allowed cone is also much less. However, when waves are present, there is very little difference in the downward radiance just below the surface at the two wavelengths for zenith angles from 40° to 60°.

VI. Radiance Within Ocean

How does the radiance at various depths within the ocean depend on the waves? Figures 23–25 show the radiance at various depths in the ocean for three solar zenith angles at $\lambda = 0.46$ μm. The sun is taken at the zenith for the curves in Fig. 23. The curves on the right are for a calm ocean. The range of zenith angles from 35° to 65° is shown in the inset. The sudden drop in the radiance at 48.4° just below the ocean surface at the boundary of the allowed cone is shown here. At an optical depth of unity below the ocean surface this discontinuity in the curve has changed into a continuous curve.

The curves on the left of Fig. 23 are for a 20-knot (37.1-km/h) wind. The radiance curve just below the surface has a much broader maximum than that for a calm ocean, as has already been noted. This broader maximum is still noticeable at an optical depth of 10 below the ocean surface. At sufficiently great depths the radiance curve must approach an asymptotic limit which is the same whether there are waves on the surface or not. Obviously an optical depth of 10 is not near this limit. The calculations of Plass *et al.*[3] and of Kattawar and Plass[4] show that this asymptotic limit is reached only at very large optical depths when the single scattering albedo $\omega_0 = 0.8$ (as is the case within the ocean at both wavelengths considered here); this is confirmed by the results presented here.

The same curves, but for a solar zenith angle of 32°, are presented in Fig. 24. When the ocean is calm, the direct solar beam is seen just beneath the ocean surface at a zenith angle of 23.33°. This maximum broadens with depth, but is still quite prominent at an optical depth of 10. At very great depth the maximum would be at the zenith. The pronounced broadening of the maxima by waves is ob-

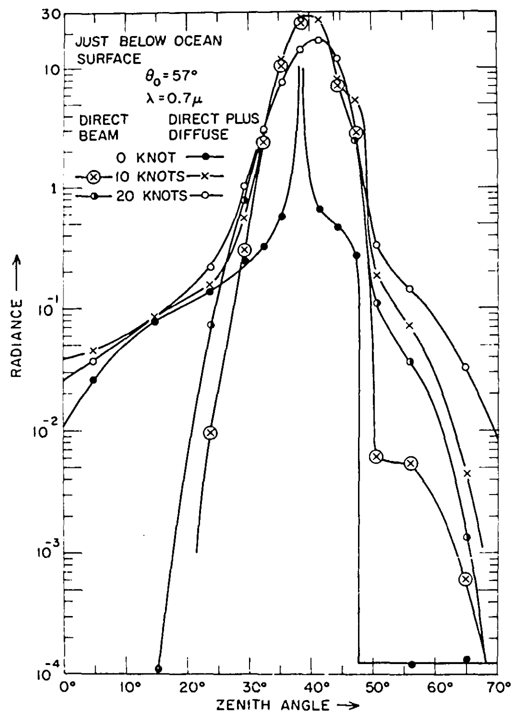

Fig. 22. Downward radiance just below ocean surface as function of zenith angle of observation for $\theta_0 = 57°$, $\lambda = 0.7$ μm, and the principal plane. See legend for Fig. 20.

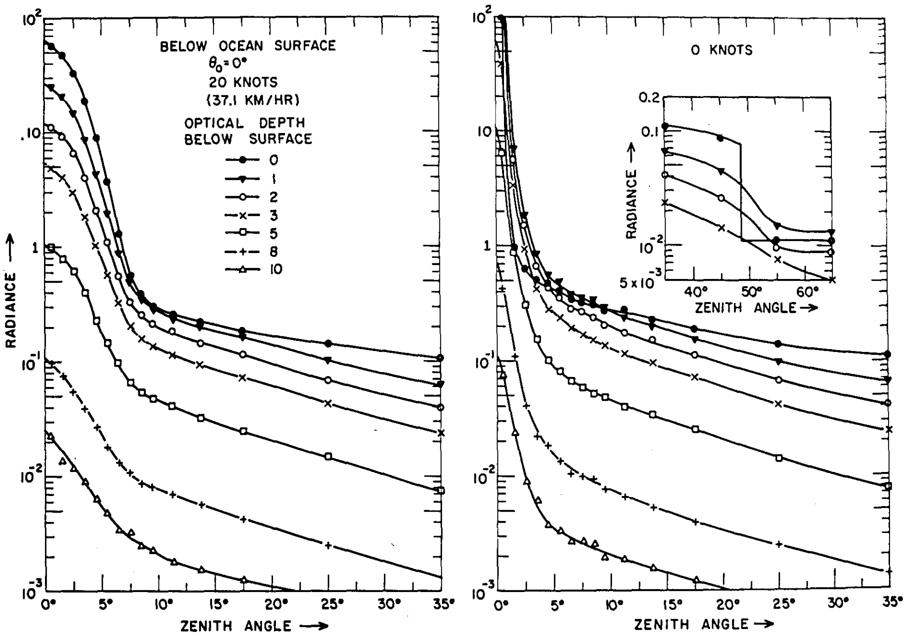

Fig. 23. Downward radiance at various depths within the ocean as a function of zenith angle of observation for $\theta_0 = 0°$. The curves on the right are for a wind speed of 0 knots, while those on the left are for 20 knots (37.1 km/h). Curves are given for the radiance at various optical depths beneath the surface from 0 to 10. The inset on the right shows the radiance for a calm ocean for zenith angles from 35° to 65°.

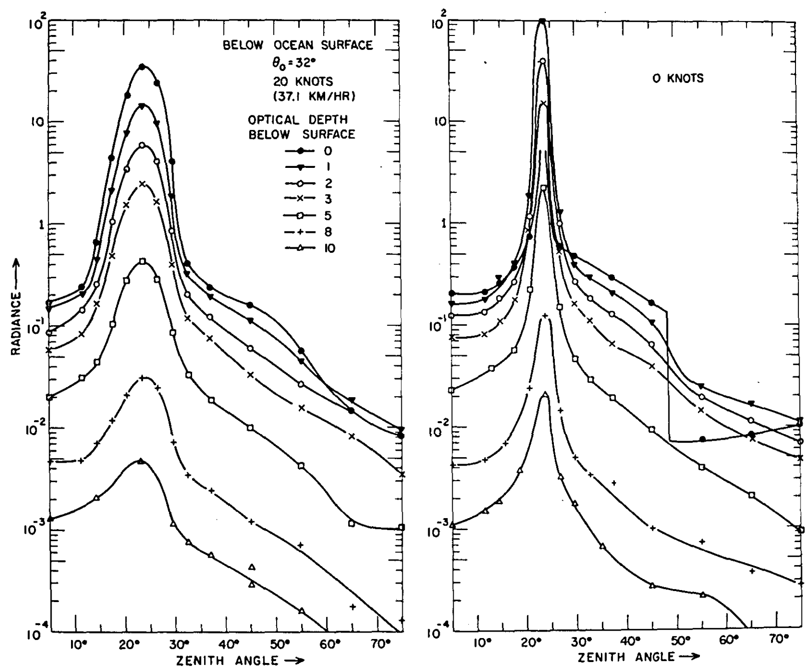

Fig. 24. Same as Fig. 23 except $\theta_0 = 32°$.

served in the curves on the left of this figure.

Figure 25 shows the same curves for a solar zenith angle of 80°. The refracted solar beam just below the surface is at 47.39°, very close to the critical angle of 48.36°. The maxima in the curves for various optical depths are much less than the corresponding ones in Fig. 24 for both a calm ocean and one with waves on the surface. There is no indication of a maximum other than at the zenith in the curve for an optical depth of 10 and a 20-knot (37.1-km/h) wind. There is, however, a fair amount of scatter in the Monte Carlo results at this depth because of the very low intensity of the light.

The variation of the radiance with depth within the ocean is shown in Fig. 26 as a function of both zenith and azimuthal angle. This figure is for a solar zenith angle of 57° and a 10-knot (18.5-km/h) wind. Curves are given at optical depths of unity and 8 beneath the ocean surface. The maximum in the radiance curve as a function of zenith angle that occurs near 38.82° for an azimuthal angle of zero decreases rapidly as the azimuthal angle increases.

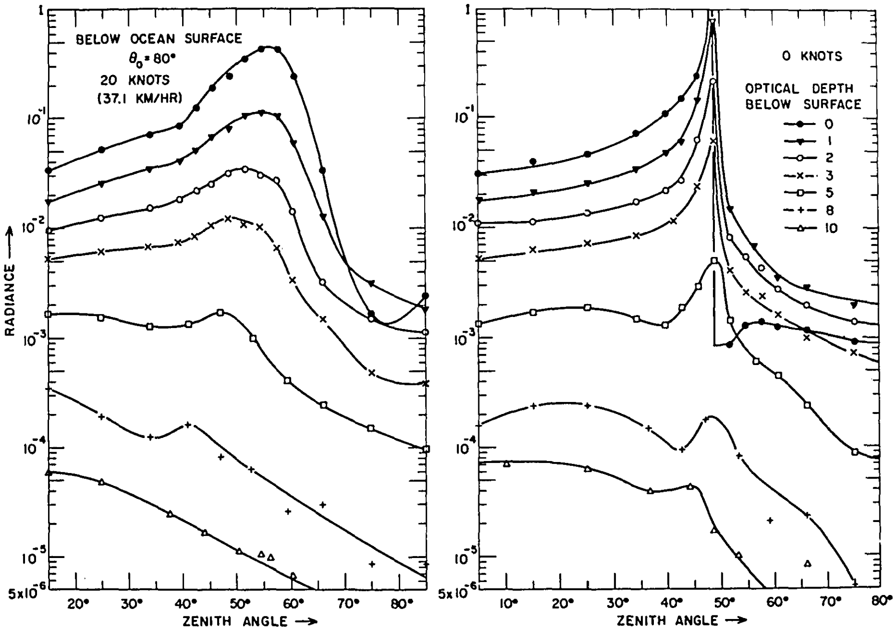

Fig. 25. Same as Fig. 23 except $\theta_0 = 80°$.

VII. Visibility of Horizon

The fact that no visible boundary can be seen at the horizon on a calm ocean is well known. A photon traveling downward from the sky at a near grazing angle to the ocean surface is virtually completely reflected at the mirror angle by a calm ocean. Thus the radiance has the same value at an angle ϵ above the horizon as at the same angle ϵ below the horizon. This is no longer true when there are waves for two reasons. (1) The sky radiance usually decreases as the angle of observation increases from the horizon upward. When there are waves the photons in the upward radiation observed at an angle ϵ just below the horizon may have been reflected from the downward radiation by a wave facet at an angle above the horizon that is considerably greater than the angle ϵ that would apply for a calm ocean. Thus the reflected sky radiance as observed near the horizon is usually less when there are waves than when there is a calm ocean. (2) Since the angle of reflection of the photon from the wave facet is no longer virtually 90°, some of the photons enter the ocean, and a smaller fraction is reflected back into the upwelling stream in the atmosphere. The fraction of photons reflected from the surface to $\theta = 90°$ drops off very rapidly from unity as the wave slope increases; it is 0.90, 0.58, and 0.35 for wave slopes of 1°, 5°, and 10°, respectively.

For both of these reasons the radiance observed just below the horizon is less than that just above. Some examples of this effect are shown in Fig. 27 for

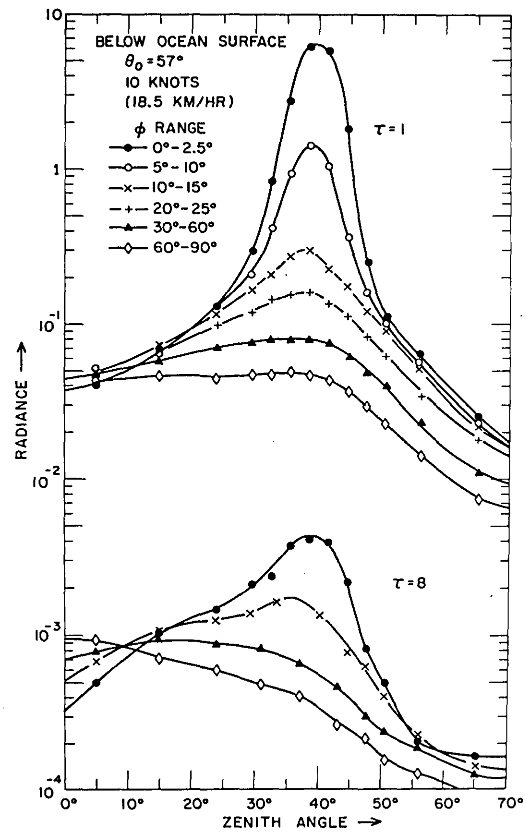

Fig. 26. Downward radiance at optical depths of 1 and 8 below the ocean surface for $\theta_0 = 57°$ and a wind speed of 10 knots (18.5 km/h). Curves are given for various values of the azimuthal angle.

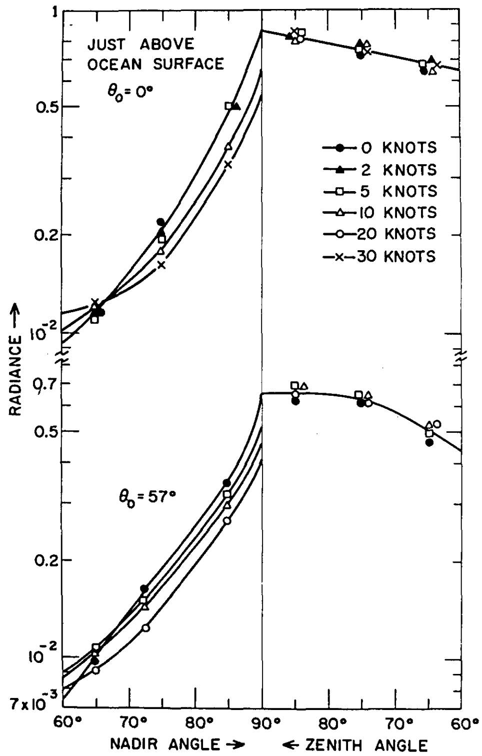

Fig. 27. Upward radiance (on left) and downward radiance (on right) in order to show variation of radiance across horizon (at center). The top curves are for $\theta_0 = 0°$ and the bottom curves for $\theta_0 = 57°$. Curves are given for various wind speeds.

$\theta_0 = 0°$ and 57°. The horizon is at the center of the figure with the upwelling radiance at the left and the downwelling at the right. When the ocean is calm, the radiance is a maximum at the horizon, but the curve is continuous with no sharp line marking the horizon. When there are waves, there is no change in the downwelling radiance near the horizon within the accuracy of these calculations. However, there is a significant change in the upwelling radiance near the horizon; it is 40% less near the horizon when a strong wind (20–30 knots) is blowing compared to a calm ocean. This creates the sharp horizon that is usually seen over the ocean on reasonably clear days.

VIII. Important Factors Just Above Surface

How much of the upwelling radiance observed just above the ocean surface comes from the direct solar beam reflected upward by the waves *(S)*, from sky radiation (photons that have been scattered in the atmosphere) reflected upward by the waves *(A)*, and from upwelling photons that have been scattered within the ocean and reenter the atmosphere (0)? Each of these factors is compared with the total radiance in Fig. 28 for two typical solar angles of $\theta_0 = 32°$ and 80° and a wind speed of 20 knots (37.1 km/h).

The contribution from (0) changes only slightly as the nadir angle varies; thus it is the greatest percentage of the total radiance at the nadir angles where the total radiance is small; about half of the photons come from (0) near the nadir. (0) does not make the major contribution to the radiance at any nadir angle for the cases considered here.

The contribution from *(S)* is largest at nadir angles near the angle for specular reflection of the direct solar beam. *(S)* makes the largest contribution to the total radiance of the three factors for all nadir angles from 44° to 90° when $\theta_0 = 80°$ and from 0° to 67° when $\theta_0 = 32°$.

The contribution from *(A)* increases rapidly as the nadir angle approaches 90° for both solar zenith angles shown here. The increase of *(A)* with nadir angle is, of course, due to the increase of the reflectance of the ocean surface as a grazing angle is approached and to the increase in the sky radiance near the horizon. *(A)* makes the largest contribution to the total radiance of the three factors for all nadir angles from 0° to 44° when $\theta_0 = 80°$ and from 67° to 90° when $\theta_0 = 32°$.

IX. Dependence of Surface Albedo on Wind

The flux of downward radiation just below the ocean surface increases as the wind speed increases. When the sun is near the horizon more radiation enters the ocean on a windy than on a calm day since the transmissivity of the direct solar ray is more for a tilted facet of a wave than for the flat surface of the calm ocean. The downward flux just below the ocean surface is shown in Table I for various wind

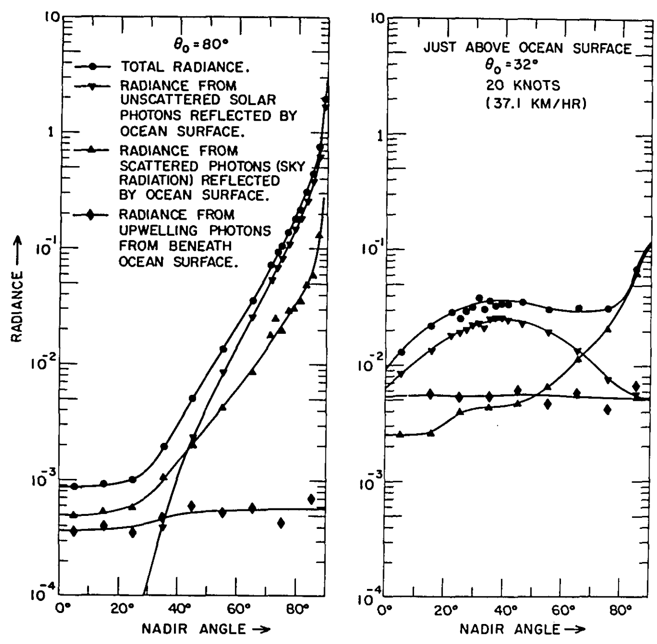

Fig. 28. Upward radiance just above ocean surface as a function of nadir angle for $\theta_0 = 80°$ (at left) and 32° (at right) and a wind speed of 20 knots (37.1 km/h). The four curves show the total radiance, the radiance from the direct solar beam as reflected by the ocean surface, the radiance from scattered photons (sky radiation) reflected by the ocean surface, and the radiance from upwelling photons from beneath the ocean surface.

Table I. Flux just below Surface and Albedo of Surface

θ	Wavelength (μm)	Wind speed knots	km/h	Flux just below surface	Albedo of surface
0°	0.46	0	0	0.864	0.0555
		10	18.5	0.870	0.0532
		20	37.1	0.871	0.0528
		30	55.6	0.874	0.0526
32°	0.46	0	0	0.837	0.0593
		10	18.5	0.840	0.0590
		20	37.1	0.847	0.0579
57°	0.46	0	0	0.740	0.0886
		10	18.5	0.751	0.0884
		20	37.1	0.758	0.0870
57°	0.70	0	0	0.835	0.0650
		10	18.5	0.841	0.0649
		20	37.1	0.848	0.0645
80°	0.46	0	0	0.478	0.142
		10	18.5	0.480	0.137
		20	37.1	0.514	0.123

speeds and solar zenith angles. When $\theta_0 = 80°$ the downward flux just below the surface is 7.5% greater for a 20-knot (37.1-km/h) wind than for a calm ocean. For the same reasons the albedo (ratio of upward flux to total downward flux) of the ocean surface decreases as the wind speed increases, being 13% less for a 20-knot wind than for a calm ocean when $\theta_0 = 80°$.

Table I shows that the downward flux just below the surface increases with wind speed, and the surface albedo decreases with wind speed at all solar angles. The variation is much smaller when the sun is nearer the zenith. For example, the downward flux just below the surface increases 1.2% when the wind increases from 0 knots to 30 knots (55.6 km/h).

Although the increase in the flux just below the surface with wind speed when the sun is near the horizon has been pointed out in the literature (Cox[14]), there does not appear to have been any previous mention of this effect for solar angles near the zenith. At first sight one would not expect this effect to occur when the sun is at the zenith, since the reflection coefficient changes very little for angles from 0° to 50° (2.1–3.4%). Since a 50° wave slope is not probable, the change in the fraction of the direct solar beam entering the ocean is small as the wind speed increases, and furthermore this effect slightly decreases this fraction. The small increases with wind speed calculated for the downward flux just below the surface when the sun is near the zenith is due to another effect, namely, that of the sky radiance near the horizon. If the sky radiance were uniform, there would be no effect. However the sky radiance has a relative maximum near the horizon, decreases farther from the horizon, and then increases again near the position of the sun. More of the sky radiance from directions near the horizon can enter the water when there are waves because of the increased transmissivity of the tilted wave facets. This is the reason that the downward flux just below the surface slightly increases with wind speed when the sun is near the zenith; correspondingly the albedo of the sea surface slightly decreases.

X. Conclusions

The radiance at various levels in the atmosphere and ocean is influenced in varying degrees by the waves on the ocean surface. This influence is small on the downward radiance within the atmosphere. On the other hand the upward radiance just above the ocean surface to the top of the atmosphere is strongly influenced by the waves, particularly for the ranges of angles around the mirror direction for a calm ocean. The changes in radiance are sufficient that the sea state might be inferred from satellite measurements.

Within the ocean the waves greatly change the downward radiance, smoothing out the abrupt transition that occurs at the edge of the allowed cone for radiation entering a calm ocean. The waves influence the downward radiation even at considerable depths within the ocean and in some cases until the diffusion or asymptotic region is reached.

These calculations explain the contrast between the sky and sea at the horizon and how it increases as the wave slope increases. It is shown that the surface albedo decreases with wind speed at all solar angles, although the effect is larger when the sun is near the horizon.

This research was supported by the Office of Naval Research through contract N00014-68-A0308-0002.

References

1. G. N. Plass, G. W. Kattawar, and F. E. Catchings, Appl. Opt. **12**, 314, 1071 (1973).
2. G. W. Kattawar and G. N. Plass, J. Quant. Spectrosc. Radiat. Transfer **13**, 1065, 1081 (1973); **15**, 61 (1975).
3. G. N. Plass, G. W. Kattawar, and J. Binststock, J. Quant. Spectrosc. Radiat. Transfer **13**, 1081 (1973).
4. G. N. Plass and G. W. Kattawar, Appl. Opt. **7**, 415 (1968).
5. G. N. Plass and G. W. Kattawar, J. Atmos. Sci. **28**, 1187 (1971).
6. G. N. Plass and G. W. Kattawar, Appl. Opt. **8**, 455 (1969).
7. G. N. Plass and G. W. Kattawar, J. Phys. Oceanogr. **2**, 249 (1972).
8. G. W. Kattawar and G. N. Plass, J. Phys. Oceanogr. **2**, 146 (1972).
9. G. W. Kattawar, G. N. Plass, and J. A. Guinn, Jr., J. Phys. Oceanogr. **3**, 353 (1973).
10. E. Raschke, Beitr. Phys. Atmos. **45**, 1 (1972).
11. H. R. Gordon and O. B. Brown, Appl. Opt. **12**, 1549 (1973).
12. L. Elterman, *UV, Visible, and IR Attenuation for for Altitudes to 50 km, 1968*, Air Force Cambridge Research Laboratories Report AFCRL-68-D153 (1968); Appl. Opt. **8**, 893 (1969).
13. C. Cox and W. Munk, J. Opt. Soc. Am. **44**, 838 (1954).
14. C. S. Cox, in *Optical Aspects of Oceanography*, N. G. Jerlov and E. S. Nielsen, Eds. (Academic, New York, 1974).